Vibration energy harvesting system with coupled bistable modules

Patrick Dorin*[a], Jinki Kim[b], K. W. Wang[a]
[a]Dept. of Mechanical Engineering, University of Michigan, Ann Arbor, MI, USA 48109-2125;
[b]Dept. of Mechanical Engineering, Georgia Southern University, Statesboro, GA, USA 30460-8046

ABSTRACT

Bistable vibration energy harvesters have been used to achieve strong energy harvesting performance over a wide frequency bandwidth. Performance of bistable energy harvesters is dependent on whether the external excitation is large enough to surpass the minimum threshold to high energy, or 'snap through' oscillations. Studies have indicated that lowering the potential energy barrier via an auxiliary unit is an effective way to ensure that high energy orbits are achieved. Recent advancements have shown that directly extracting energy from an auxiliary unit used to dynamically lower the potential barrier of a bistable energy harvester can enhance performance. However, there remains an unexplored opportunity for further improvement by incorporating nonlinearity into the auxiliary harvesting element. Thus, to advance the state of the art, this research introduces an energy harvesting system composed of a bistable cantilever harvester magnetically coupled to an auxiliary nonlinear harvesting element. An analysis of the system potential energy indicates that the additional nonlinear characteristics of the coupled harvesting element can enable tailoring of the potential energy profile such that quad-stability, or multi-directional bistability, can be achieved. Investigation of the quasi-static potential energy trajectory of the proposed device indicates that the number of stable states, height of the potential energy barrier, and snap through amplitude may all be tailored through consideration of the effective linear stiffness of the nonlinear harvesting unit. Numerical simulations of the system dynamics indicate that the additional nonlinearity incorporated into the coupled system improves broadband harvesting performance.

Keywords: energy harvesting, nonlinear, bistable, coupled, adaptive potential, piezoelectric, broadband, potential energy

1. INTRODUCTION

The current state of battery technology can result in high maintenance or replacement costs, environmental hazards, and an inability to miniaturize electrical devices due to a limited power density.[1] With these limitations in mind, vibration energy harvesting is being studied as a method to replace or recharge conventional batteries in a variety of applications. Examples of applications where vibration energy harvesting is viewed as a viable power source include, but are not limited to, structural health monitoring,[2,3] biomedical implantable devices,[4] and unmanned aerial vehicles.[5,6] Initial vibration energy harvesting systems operated on the concept of linear resonance, and thus performed best for environments with invariant, single-frequency excitations that can be known beforehand.[1] However, the performance of conventional linear energy harvesters can degrade for many practical applications, which often operate in environments where ambient excitations are time-varying or cover a broad frequency bandwidth. Thus, a variety of methods have been studied to improve the robustness of performance to a broad set of external excitation conditions. Two methods that have been demonstrated to improve system performance over a broad frequency bandwidth include multimodality,[7–9] which involves the addition of multiple modes of harvesting that perform well under different excitation conditions, and the deliberate introduction of nonlinearity,[10–12] which leverages the wide frequency region of nonlinear response.

A particular type of nonlinearity that has been heavily investigated is bistability, since bistable energy harvesters possess the capability to undergo high amplitude oscillations (known as interwell or snap-through oscillations) for a wide range of external excitation conditions.[11,13–21] A bistable energy harvester contains two stable equilibria that are separated by a central unstable equilibrium position that constitutes a potential energy barrier (Table 2- inset figure). When subjected to small amplitude excitations, bistable energy harvesters undergo low-energy oscillations about one of the two stable equilibrium positions, known as intrawell response.[22] If the external excitation amplitude is large enough to overcome the potential energy barrier which separates the two stable states, the harvester exhibits high-energy oscillations between the two stable states known as interwell response.[22] Thus, the potential energy barrier serves as a threshold that must be surpassed by the amplitude of the external excitation to achieve interwell response. When the high-energy interwell

*Corresponding Author: Patrick Dorin, email: pdorin@umich.edu

response is activated, studies have shown that bistable energy harvesters outperform traditional linear harvesters for broadband harmonic[23,24] and stochastic[12,25] external excitation conditions. To ensure that the high-energy interwell oscillations are attainable for the widest possible set of excitation conditions (broadband excitation conditions), methods have been proposed to lower the potential energy barrier without reducing the distance between stable equilibrium points, also known as the snap through amplitude (Table 2- inset figure). Static mechanisms used to achieve this goal include the addition of stable states (e.g. tri-stable, quad-stable),[26,27] rotatable magnets,[28] and extra magnets[29] to the conventional bistable harvester. These static mechanisms reduce the potential energy barrier to a level that remains constant throughout system operation, and have been shown to facilitate interwell oscillations and improve performance over a conventional bistable system. Alternatively, mechanisms have been developed that dynamically raise and lower the barrier during system operation, expanding the design space of achievable potential energy characteristics and creating an adaptive potential energy function. Active mechanisms, such as an electromagnet,[30,31] have been demonstrated to improve broadband performance by dynamically changing the potential barrier height using an external power source and simple control input. To avoid the parasitic power required by the active methods, the fixed magnet of a conventional bistable system has been replaced by a magnet-spring linear oscillator to dynamically lower the potential energy barrier using a passive mechanism.[32–38] Apart from successfully lowering the potential energy barrier, recent advancements have incorporated multi-degree-of-freedom (MDOF) energy harvesting into these adaptive potential systems, and have shown that there is potential to further improve broadband performance by directly extracting additional energy from the linear passive mechanism that is used to lower the potential energy barrier.[39] However, there remains an unexplored opportunity to advance the state of the art by incorporating nonlinearity into the passive harvesting mechanism that is utilized to lower the potential energy barrier of a conventional bistable harvester. In this report, an energy harvesting system comprised of a bistable cantilever that is magnetically coupled to a nonlinear clamped-clamped beam is presented. A pre-compressed linear spring is connected in parallel to the nonlinear clamped-clamped beam to introduce an asymmetric (non-zero) equilibrium point for the local potential energy function. The proposed system is configured in a manner such that its adjustable potential energy profile can be exploited to synergistically lower the potential energy barrier to energetic interwell motion and broadly enhance harvesting bandwidth through MDOF bistability. While the rich dynamics of coupled bistable systems have been explored previously, the primary design criteria has been to obtain strong performance in multiple frequency bands from coupled conventional symmetric bistable devices and analysis has focused on system dynamics at distinct modal frequencies.[40–46] The energy harvesting system proposed here is comprised of a conventional symmetric bistable harvester magnetically coupled to an asymmetric nonlinear energy harvesting element, as opposed to a conventional symmetric bistable or linear element. As a result of the unique characteristics of the asymmetric nonlinear element, the harvesting system will not only be capable of harvesting energy in multiple frequency bands, but also better harness MDOF interwell dynamics through a highly adaptive potential energy function.

The governing equations for the proposed system, which harvests energy via piezoelectric transducers, are derived using the extended Hamilton's principle and then discretized using the assumed modes method. The working principle is then presented through a comprehensive potential energy analysis which includes investigation of the quasi-static potential energy trajectories of the proposed system and the current state of the art across a potential energy surface. Numerical simulations of the dynamic governing equations are then conducted to demonstrate the efficacy of the proposed device with regards to energy harvesting over a wide excitation bandwidth. Finally, overall discussion and conclusion are presented.

2. SYSTEM DESCRIPTION AND MATHEMATICAL MODEL

2.1 System description

The proposed system is comprised of a cantilever beam with tip magnet (magnet 1) that is axially aligned with a magnet (magnet 2) attached to the midpoint of a clamped-clamped beam that is connected in parallel to a pre-compressed linear spring (Figure 1a). Magnet 1 and magnet 2 contain opposing polarities, creating a repulsive magnetic force that induces nonlinearity in the cantilever beam. The distance between magnet 1 and magnet 2 is defined as small enough such that the repulsive magnetic force can overcome the cantilever beam's elastic restoring force, resulting in a pitchfork bifurcation and two stable static equilibria (bistable).[21,23,39,40] Attached to the bistable cantilever beam are two piezoelectric transducers for energy conversion. The clamped-clamped beam with magnet fixed to the center point ($z = 0$) is axially-loaded to provide nonlinearity. This element lowers the potential energy barrier for the bistable cantilever beam as the cantilever

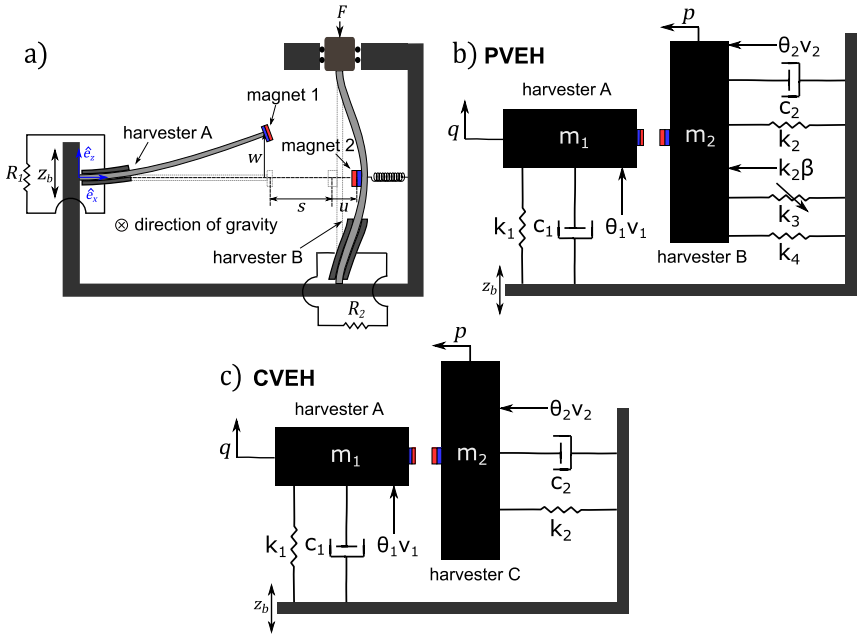

Figure 1. Schematic (a) and lumped parameter model (b) of the proposed magnetically coupled energy harvester with bistable harvesting element (harvester A) and nonlinear harvesting element (harvester B). Lumped parameter model (c) of the current state of the art, a magnetically coupled energy harvester with bistable harvesting element (harvester A) and linear harvesting element (harvester C).

passes through the center unstable equilibrium point ($w = 0$). Sufficient preload (F) is applied to the clamped-clamped beam to induce buckling, while the pre-compressed linear spring acts to provide a balancing force in the negative x-direction ($-x$) that counteracts the magnetic coupling force acting on magnet 2 in the positive x-direction ($+x$). The magnitude of pre-compression of the linear spring is modulated by varying its unstretched equilibrium point, which is to the left of the centerline of the clamped-clamped beam, using an offset parameter β. Two piezoelectric transducers are also applied to the clamped-clamped beam for energy conversion. The piezoelectric transducers attached to the cantilever and clamped-clamped beams are connected to external resistive loads R_1 and R_2, respectively, for energy harvesting from an external base excitation z_b acting transversely to the length of the cantilever beam. In summary, the proposed energy harvesting system is comprised of a bistable piezoelectric harvesting element (harvester A) that is magnetically coupled to an asymmetric nonlinear piezoelectric harvesting element (harvester B). For the purpose of this investigation, the previous work in MDOF harvesting systems with adaptive potential energy, which has focused on a bistable cantilever harvester coupled to a linear harvesting element,[39] will be treated as the current state of the art. A lumped parameter model (Figure 1c) of a general representation of the current state of the art, comprised of a bistable harvesting element (harvester A) magnetically coupled to a linear harvesting element (harvester C), is also provided. To be concise, the proposed energy harvesting system (composed of harvester A and harvester B) will be referred to as PVEH, while the system representing the current state of the art (composed of harvester A and harvester C) will be referred to as CVEH.

2.2 Mathematical model

A mathematical model of the continuous system depicted in Figure 1a is derived from the extended Hamilton's Principle,[47,48] and deformations are assumed small enough such that Euler-Bernoulli beam theory[23,47] and theory of linear piezoelectricity[47,49] can be applied. Perfectly conductive piezoelectric layers and a uniform electric field are assumed for all piezoelectric elements. A lumped parameter model is developed by using the assumed modes method, where the transverse displacements of the cantilever beam (w) and the clamped-clamped beam (u) are expanded into a superposition of N trial functions:

$$w(x,t) = \sum_{i=1}^{N} \phi_i(x) q_i(t) \tag{1a}$$

$$u(z,t) = \sum_{i=1}^{N} \psi_i(z) p_i(t) \tag{1b}$$

where $\phi_i(x)$ and $\psi_i(z)$ are the trial functions and $q_i(t)$ and $p_i(t)$ are time-dependent generalized coordinates. For the purpose of this discussion, it is assumed that the fundamental mode dominates response for both beams. Thus, the trial functions used are the first modal function of the uniform cantilever beam with tip mass[49] (harvester A) and that of the uniform clamped-clamped beam[18,33] (harvester B). The resulting discretized governing equations of the PVEH are given as[18,21,33,40]:

$$m_1\ddot{q}(t) + c_1\dot{q}(t) + k_1 q(t) + F_q + \Theta_{p1} V_{p1}(t) = -B_f \ddot{z}_b(t) \tag{2a}$$

$$\Theta_{p1}\dot{q}(t) - \frac{1}{2} C_{p1}\dot{V}_{p1}(t) = \frac{V_{p1}(t)}{R_1} \tag{2b}$$

$$m_2\ddot{p}(t) + c_2\dot{p}(t) + k_4 p(t) + k_3 p(t)^3 + k_2(p(t) - \beta) + F_p + \Theta_{p2} V_{p2}(t) = 0 \tag{2c}$$

$$\Theta_{p2}\dot{p}(t) - \frac{1}{2} C_{p2}\dot{V}_{p2}(t) = \frac{V_{p2}(t)}{R_2} \tag{2d}$$

where $\ddot{z}_b = p \cos 2\pi f_e t$ is the harmonic base excitation of amplitude p and frequency f_e; $V_{p1}(t)$ is the voltage response of harvester A; $V_{p2}(t)$ is the voltage response of harvester B; F_q and F_p are the magnetic forces acting on magnet 1 and magnet 2, respectively; B_f is a forcing factor that accounts for the inertial loading of the cantilever beam and proof mass due to the external base excitation;[47,50] and all other terms are constants defined in Table 1. The overdot represents a time derivative. Equations 2a and 2b represent the dynamics of harvester A, while Equations 2c and 2d represent the dynamics of harvester B, with the magnetic forces F_p and F_q representing the coupling terms between the two harvesters. The lumped parameter model of the PVEH associated with Equations 2a-2d is shown in Figure 1b.

For the mathematical model of the CVEH, the governing equations for harvester A (Equations 2a and 2b) and the second harvesting circuit (Equation 2d) remain unchanged (see Equations 3a, 3b, 3d), while the parameters associated with the nonlinearity of harvester B of the PVEH (k_4,k_3,β) are set to zero to represent the dynamics of linear harvester C of the CVEH (Equation 3c).

Table 1. Definition of constants for mathematical model, potential energy analysis, and system dynamics numerical investigation

Symbol	Parameter	Value	Symbol	Parameter	Value
Harvester A (PVEH and CVEH)			**Harvester B (PVEH)**		
m_1	Effective mass	10.4 g	m_2	Effective mass	100 g
c_1	Effective damping coefficient	0.008 Ns/m	c_2	Effective damping coefficient	0.008 Ns/m
k_1	Effective linear stiffness	41.6 N/m	k_2	Linear stiffness, pre-compressed spring	404 N/m
θ_{p1}	Electromechanical coupling	165 μN/V	k_3	Effective nonlinear stiffness, clamped-clamped beam	200 MN/m^3
C_{p1}	Capacitance	21.5 nF	k_4	Effective linear stiffness, clamped-clamped beam	-525 N/m
R_1	External resistive load	200 kΩ	β	Offset term, pre-compressed spring	-0.5 mm
Harvester C (CVEH)			θ_{p2}	Electromechanical coupling	940 μN/V
All parameters identical to harvester B except: $k_3 = k_4 = \beta = 0$			C_{p2}	Capacitance	89.9 nF
			R_2	External resistive load	200 kΩ

The governing equations for the CVEH are thus given as:

$$m_1\ddot{q}(t) + c_1\dot{q}(t) + k_1 q(t) + F_q + \Theta_{p1}V_{p1}(t) = -B_f\ddot{z}_b(t) \tag{3a}$$

$$\Theta_{p1}\dot{q}(t) - \frac{1}{2}C_{p1}\dot{V}_{p1}(t) = \frac{V_{p1}(t)}{R_1} \tag{3b}$$

$$m_2\ddot{p}(t) + c_2\dot{p}(t) + k_2 p(t) \ + F_p + \Theta_{p2}V_{p2}(t) = 0 \tag{3c}$$

$$\Theta_{p2}\dot{p}(t) - \frac{1}{2}C_{p2}\dot{V}_{p2}(t) = \frac{V_{p2}(t)}{R_2} \tag{3d}$$

where $V_{p2}(t)$ is the voltage response of harvester C and all other parameters are defined in Table 1. The lumped parameter model of the CVEH associated with Equations 3a-3d is shown in Figure 1c. The magnetic forces acting on magnet 1 (F_q) and magnet 2 (F_p) are defined by modeling magnet 1 and magnet 2 as point dipoles with magnetic moments (which give a measure of magnetic strength) defined as[23,51]:

$$\mu_1 = M_1V_1\cos\theta(L_1)\hat{e}_x + M_1V_1\sin\theta(L_1)\hat{e}_z \tag{4a}$$

$$\mu_2 = -M_2V_2\hat{e}_x \tag{4b}$$

with $\theta(L_1)$ being the rotation angle of the cantilever tip; μ_1, μ_2 being the magnetic moment vectors, M_1 and M_2 the magnetization vectors, and V_1 and V_2 the material volumes of magnet 1 and magnet 2, respectively.[51] The magnetization vectors M_1 and M_2 can be approximated as $M_{1,2} = \frac{B_r}{\mu_0}$, where $\mu_0 = 4\pi \times 10^{-7}$ H/m is the permeability of free space and B_r is the residual flux density of each magnet. For this study, $M_1 = M_2 = 1.2$ MA/m, $V_1 = 1.2 \times 10^{-7}$ m^3, and $V_2 = 7.8 \times 10^{-7}$ m^3. The magnet attached to harvester A (magnet 1) is designed smaller to avoid over-rotation of the cantilever beam tip, which can cause excess strain in the piezoelectric transducers attached at the root of the cantilever. The magnet attached to harvester B (magnet 2) is designed larger to add inertia to the midpoint of the clamped-clamped beam and amplify dynamic response. The magnetic forcing varies instantaneously as a function of the distance from the source of μ_2 to the source of μ_1 which is given as:

$$\vec{r}_{12} = -(s + u(L_2/2))\hat{e}_x + \left[w(L_1) + \frac{1}{2}t_{m1}\theta(L_1)\right]\hat{e}_z \tag{5}$$

where s is the distance between the dipoles in their respective equilibrium states (see Figure 1a), t_{m1} is the thickness of magnet 1, $w(L_1)$ is the tip displacement of the cantilever beam, $u(L_2/2)$ is the midpoint displacement of the clamped-clamped beam, and $\theta(L_1)$ is the rotation angle of the cantilever beam tip. In this study $s = 24$ mm and $t_{m1} = 1.6$ mm. The magnetic field B_{12} generated by magnet 1 at the location of magnet 2 and corresponding magnetic potential energy U_m are defined as:

$$B_{12} = -\frac{\mu_0}{4\pi}\nabla\frac{\mu_1 \cdot r_{12}}{\|r_{12}\|_2^3} \tag{6}$$

$$U_m = -B_{12} \cdot \mu_2 = \frac{\mu_0}{4\pi}\left(\frac{\mu_1 \cdot \mu_2}{\|r_{12}\|_2^3} - 3\frac{(\mu_1 \cdot r_{12})(\mu_2 \cdot r_{12})}{\|r_{12}\|_2^5}\right) \tag{7}$$

And the equivalent magnetic forces are calculated as:

$$F_q(q,p) = \frac{\partial U_m}{\partial q}, F_p(q,p) = \frac{\partial U_m}{\partial p} \tag{8a, 8b}$$

The total output power P_{tot} for the PVEH is the aggregate of the instantaneous power generated from harvester A (P_1) and harvester B (P_2) under external excitation. Similarly, the total output power of the CVEH is the aggregate of the power generated by harvester A (P_1) and harvester C (P_2). The general form of total output power is given as:

$$P_{tot} = \sum_{i=1}^{2} P_i = \sum_{i=1}^{2} \frac{1}{T}\int_0^T \frac{V_{pi}^2}{R_i}dt \tag{9}$$

where the measurement period T is defined as large enough in relation to the base excitation period ($1/f_e$) such that the system is operating in a regime of steady-state behavior.

3. POTENTIAL ENERGY ANALYSIS

The total potential energy of the PVEH is defined as the summation of the magnetic potential energy (Equation 7) and the strain energies of harvester A and harvester B:

$$U_{PVEH}(q,p) = U_m + \overbrace{\frac{1}{2}k_1q^2}^{U_{harvester\,A}} + \overbrace{\frac{1}{2}k_2p^2 - k_2\beta p + \frac{1}{2}k_4p^2 + \frac{1}{4}k_3p^4}^{U_{harvester\,B}} \tag{10}$$

Total potential energy of the CVEH is defined as the summation of the magnetic potential energy and the strain energies of harvester A and harvester C:

$$U_{CVEH}(q,p) = U_m + \overbrace{\frac{1}{2}k_1q^2}^{U_{harvester\,A}} + \overbrace{\frac{1}{2}k_2p^2}^{U_{harvester\,C}} \tag{11}$$

Figure 2 depicts the potential energy surfaces for the PVEH (Figure 2a) and the CVEH (Figure 2b), as a function of the displacements of the tip of the bistable cantilever beam $w(L_1)$ and the midpoint of the nonlinear clamped-clamped beam $u(L_2/2)$. The solid lines placed directly onto the potential energy surfaces in Figure 2 represent the potential energy trajectory of each system for a full cycle of motion of the bistable cantilever, and are generated by quasi-statically changing the position of the bistable cantilever $w(L_1)$, and solving the static form of the governing equations for the corresponding location of the clamped-clamped midpoint $u(L_2/2)$. The level lines shown below the potential energy surfaces indicate increasing potential energy with increasing brightness. Local minima, which indicate stable system states, are enclosed in level lines that are blue ovals. The parameters for harvester A are identical in both the PVEH and CVEH. The linear spring constant k_2 and mass m_2 parameters for harvester C of the CVEH are determined through a parametric analysis (see Section 4.1: CVEH performance maximization) with the objective of maximum power generation for a given set of excitation conditions. For harvester B of the PVEH, the linear spring constant for the pre-compressed linear spring k_2 is selected to match the linear spring constant of the CVEH, the linear spring stiffness of the clamped-clamped beam under preload k_4 is selected such that harvester B is buckled and exhibits bistability ($k_2 + k_4 < 0$), the nonlinear stiffness k_3 is selected to be in the range of representative values from similar systems,[18,33,52] and the magnitude of the asymmetry term β is selected to be less than the magnitude of the theoretical stable equilibria of the nonlinear clamped-clamped element under preload ($|\beta| < \sqrt{|k_2 + k_4|/k_3}$). All parameters used to generate the potential energy surfaces for the PVEH and the CVEH are listed in Table 1.

The potential energy surface for the PVEH (Figure 2a) contains four local minima (stable states), indicating bistability in both of the harvesting elements (harvester A and harvester B), or quad-stability for the entire system. On the other hand, the potential energy surface for the CVEH (Figure 2b) contains just two local minima that are symmetrically aligned about $w(L_1) = 0$ mm, indicating bistability only in harvester A, while harvester C exhibits a monostable potential. Figure 3 contains projections of the quasi-static potential energy trajectories (solid lines on the potential energy surfaces in Figure 2) solely as a function of cantilever tip displacement $w(L_1)$ (Figure 3a) or clamped-clamped midpoint displacement $u(L_2/2)$ (Figure 3b). Each projection corresponds to the quasi-static potential energy trajectory for an individual harvesting subsystem. The potential energy trajectories for harvester A of the PVEH, harvester A of CVEH, and a conventional bistable system with fixed magnet are shown in Figure 3a, while the trajectories for harvester B of the PVEH and harvester C of the CVEH are shown in Figure 3b. The potential energy barrier, or the maximum difference in potential energy between a stable state (local minima) and center unstable state (local maximum), and snap through amplitude, or distance between stable states, are measured for each individual subsystem and listed in Table 2. Figure 3a contains the potential energy trajectory pertaining to harvester A ($w(L_1)$ – direction) of both the PVEH and CVEH. It is observed that both systems lower the potential energy barrier for the bistable cantilever (harvester A for both PVEH and CVEH) when compared to a conventional bistable harvester with magnet 2 fixed at $u(L_2/2) = 0$. Harvester A is bistable for both the PVEH and CVEH; however, harvester A of the PVEH achieves a lower potential barrier height (60 μJ compared to 70 μJ for CVEH) accompanied with a larger snap through amplitude (18.8 mm compared to 13.8 mm for CVEH). A lower barrier height for the PVEH facilitates interwell oscillations for a larger range of excitation conditions, while a larger snap through amplitude enables higher amplitude motion and greater power generation. In addition, Figure 3b confirms that the

PVEH, in its coupled form, achieves bistability in harvester B (blue line), while harvester C of the CVEH is confined to a monostable potential (red line). Thus, inclusion of asymmetry and nonlinearity into harvester B of the PVEH allows the fully coupled system to achieve MDOF bistability (quad-stability) and encourages high amplitude motion in harvester B that is not present in the linear harvester C of the CVEH.

Next, the effect of varying the linear spring stiffness k_2 of the pre-compressed spring in harvester B of the PVEH is studied. Figures 2c and 2d contain the potential energy surfaces for the PVEH with different linear spring stiffness k_2 values as a function of $w(L_1)$ and $u(L_2/2)$. A k_2 value of 0 N/m is selected to evaluate the potential energy function for a PVEH with no asymmetry from the pre-compressed spring, and thus the nonlinear harvesting element is effectively a conventional symmetric bistable clamped-clamped beam with no parallel spring attachment. For a k_2 value of 0 N/m, four local minima (quad-stability) still exist in the PVEH and harvester B remains bistable (Figure 2c). However, system stable states develop asymmetry along the $u(L_2/2)$ - direction, as the local minima that are positive in $u(L_2/2)$ have a much lower potential energy U than the local minima that are negative in $u(L_2/2)$. For high k_2= 750 N/m, the pre-compressed spring exhibits such influence that the PVEH loses two potential energy minima, making the entire system only bistable (Figure 2d), like the CVEH. The resulting two potential energy minima are centered around the unstretched equilibrium of the pre-compressed spring, β = -0.5 mm. Evaluating the quasi-static potential energy trajectory of harvester A (Figure 3a) indicates potential energy barriers in both high and zero k_2 configurations that are much greater than the 60 μJ barrier for the PVEH with k_2 = 404 N/m (190 μJ for k_2= 0 N/m and 230 μJ for k_2= 750 N/m). These high potential energy barriers would inhibit energetic interwell oscillations of harvester A, thus reducing broadband power generation. Evaluating the potential energy

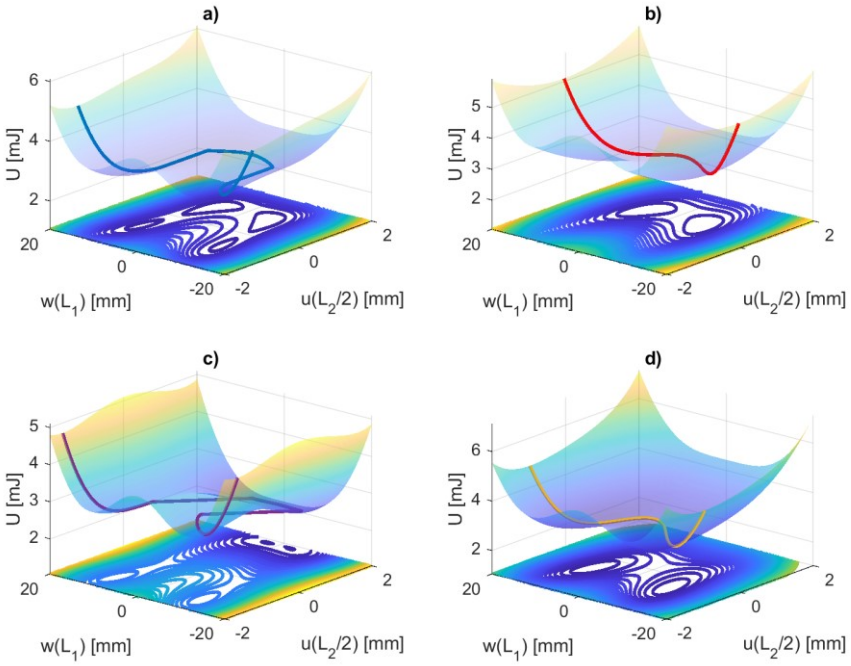

Figure 2. Potential energy surfaces for (a) PVEH with k_2 = 404 N/m; (b) CVEH with k_2 = 404 N/m; (c) PVEH with k_2 = 0 N/m; (d) PVEH with k_2 = 750 N/m. Potential energy U given as function of displacements of cantilever beam tip $w(L_1)$ and clamped-clamped beam midpoint $u(L_2/2)$. Solid lines on each surface represent quasi-static potential energy trajectories for each system. Level lines below the surfaces indicate increasing potential energy U with increasing brightness.

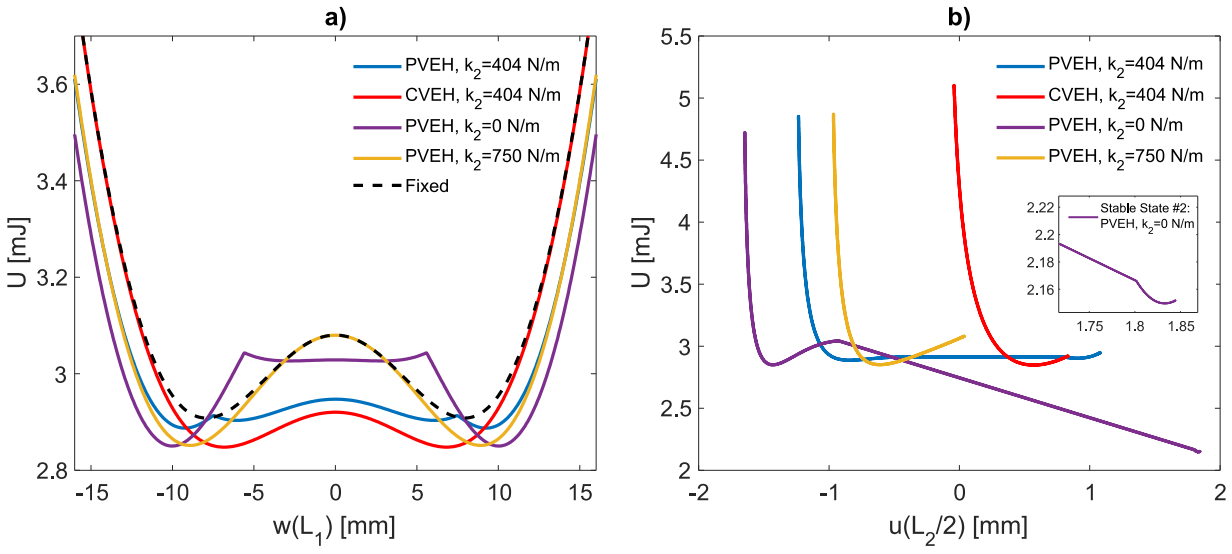

Figure 3. Projection of quasi-static potential energy trajectories onto the (a) $w(L_1) - U$ plane and the (b) $u(L_2/2) - U$ plane

Table 2. Measurements for quasi-static potential energy analysis

		Harvester A (Figure 3a)		Harvester B (PVEH); Harvester C (CVEH) (Figure 3b)		Measurement Explanation: Potential Energy Barrier and Snap Through Amplitude for Bistable System. All Measurements taken from Figures 3a and 3b
Harvesting System (line color in Figures 2,3)	**Linear Spring Stiffness, k_2**	**Snap Through Amplitude**	**Potential Energy Barrier**	**Snap Through Amplitude**	**Potential Energy Barrier**	
PVEH (Blue)	404 N/m	18.8 mm	60 μJ	1.82 mm	26 μJ	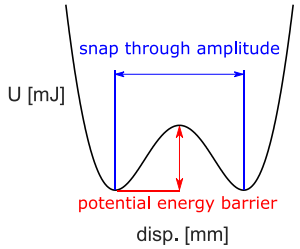
CVEH (Red)	404 N/m	13.8 mm	70 μJ	←Monostable→		
PVEH (Purple)	0 N/m	20.0 mm	190 μJ	3.26 mm	893 μJ	
PVEH (Yellow)	750 N/m	17.8 mm	230 μJ	←Monostable→		
Conventional Bistable (Black dashed)	∞ (fixed)	16.0 mm	170 μJ	←N/A (Fixed)→		

of harvester B, Figure 3b shows that selecting a conventional symmetric bistable clamped-clamped element (purple line, k_2 = 0 N/m) for harvester B leads to a large potential energy barrier between stable states (893 μJ compared to 26 μJ for k_2= 404 N/m). This large potential barrier means that the dynamic response of harvester B would likely be confined to the lower energy stable state centered at $u(L_2/2)$ = 1.83 mm (see inset "Stable State 2" in Figure 3b, small dark blue oval level lines in Figure 2c), and thus be of the small amplitude intrawell regime. On the other hand, selecting a large k_2 = 750 N/m (yellow line) confines oscillations of harvester B to a monostable potential. Both high and zero k_2 scenarios thus limit high amplitude motion and potential broadband power generation from harvester B. Therefore, addition of asymmetry through the pre-compressed linear spring in the nonlinear harvesting element is justified, and care must be taken to select a k_2 that will enable bistability for harvesters A and B with a large snap through amplitude and low potential energy barrier height.

In summary, the quad-stability of the PVEH can be designed to facilitate MDOF high amplitude motion by lowering the potential energy barrier while maintaining a large snap-through amplitude in both the $w(L_1)$ and $u(L_2/2)$ directions. This raises the possibility that high energy interwell oscillations of either harvester subsystem (A or B) may then trigger high energy interwell oscillations of the other, which would increase harvesting performance. Moreover, the addition of two

stable states when compared to conventional adaptive potential (CVEH)[39] or previously studied magnetically coupled bistable systems[40–46] engenders the possibility for harvesting enhancement via rich dynamics corresponding to the multitude of potential phase-dependent[40] intrawell and interwell dynamic trajectories between the four stable states.

4. SYSTEM DYNAMICS NUMERICAL INVESTIGATION

The dynamic response and energy harvesting performance of the PVEH under external excitation are evaluated by numerical simulations of the governing equations (Equation 2). The effectiveness of the PVEH is evaluated by comparison with dynamic simulations for the performance of the CVEH (Equation 3). The values listed in Table 1 are used for the numerical study. A range of harmonic excitations are applied to the system, with a two-dimensional excitation domain of 2 to 12 Hz and 0.5 to 8 ms^{-2} selected to match the frequency bandwidth and amplitude of many ambient excitations found in practice.[1–3,53] 10 simulations are conducted for each excitation condition (frequency-amplitude pairing) and the average power generation $P_{avg-f_e,p}$ from the 10 simulations is calculated. Each simulation has randomized initial conditions, with their range covering the stable system equilibria. Aggregate power generation $P_{aggregate}$ for the entire excitation frequency-amplitude domain is then calculated for a measure of broadband harvesting performance:

$$P_{aggregate} = \sum_{f_e} \sum_{p} P_{avg-f_e,p}\,;\;\; f_e = 2 - 12\ Hz;\;\; p = 0.5 - 8\ m/s^2 \tag{13}$$

where f_e is the excitation frequency, p is the excitation amplitude, and $P_{avg-f_e,p}$ is the average power harvested for 10 simulations of a specific excitation frequency-amplitude ($f_e - p$) pairing. The performance of the CVEH is maximized for the prescribed excitation domain and described in Section 4.1. An equivalent PVEH is evaluated against the maximized CVEH and discussed in Section 4.2.

4.1 CVEH performance maximization

The broadband performance of the CVEH for the chosen excitation domain is maximized through parametric analysis of the effective mass m_2 and linear spring stiffness k_2 system parameters. Effective mass m_2 and linear spring stiffness k_2 of harvester C of the CVEH are chosen as design variables because they have been identified as critical to system performance in previous studies regarding the current state of the art.[32,34,39] The parametric study indicates that the maximum achievable system performance for the given excitation domain is $P_{aggregate} = 333$ mW for m_2 = 0.1 kg and k_2= 404 N/m. Figure 4 shows the aggregate power generation $P_{aggregate}$ of the CVEH as a function of m_2 and k_2, with increasing brightness indicating increasing aggregate power. The region of maximum performance (yellow) is enclosed between the lines of constant linear natural frequency $f_{n2} = \frac{1}{2\pi}\sqrt{k_2/m_2}$ = 18 Hz and f_{n2} = 6 Hz, with top performance located along $f_{n2} = 10$ Hz. This feature of the system performance indicates that $P_{aggregate}$ is dependent on f_{n2} of harvester C in the CVEH.

4.2 PVEH vs. CVEH

The performance of the PVEH is analyzed by adding asymmetry and nonlinearity features to the CVEH with maximized performance developed in Section 4.1. Thus, the parameters k_2 = 404 N/m and m_2 = 0.1 kg, which maximize the

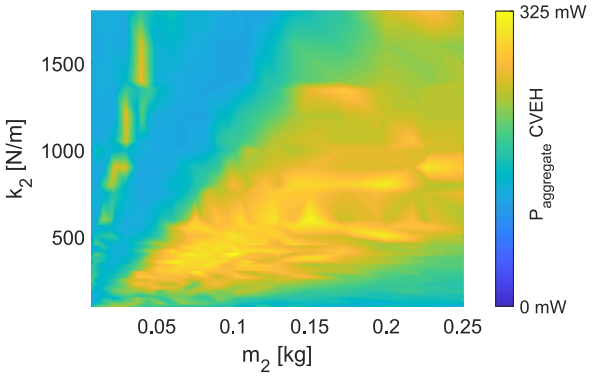

Figure 4. $P_{aggregate}$ of CVEH as a function of effective mass m_2 and effective linear stiffness k_2. More power indicated by increasing brightness.

performance of the CVEH, are selected for harvester B of the PVEH, to obtain a fair comparison between the two systems. All other system parameters for the PVEH are defined as identical to the CVEH, with the exception of the additional terms in harvester B of the PVEH associated with its asymmetric nonlinearity (k_3, k_4, β). Figure 5 shows the average harvested power of both the CVEH (Figure 5a) and PVEH (Figure 5b) as a function of base excitation frequency and amplitude. More harvested power is indicated by increasing brightness. It is evident from comparison of Figures 5a and 5b that the PVEH (Figure 5b) exhibits strong performance over a larger region of excitation characteristics than the maximized CVEH (Figure 5a). In fact, results of the numerical simulations show that the PVEH improves broadband performance by 25% when compared to the CVEH with maximized harvested power ($P_{aggregate}$ = 417 mW for PVEH and 333 mW for CVEH).

Decomposing each system and analyzing the performance of each subsystem shows that harvester A of the CVEH achieves a $P_{aggregate-harvester\ A}$ of 159 mW, while the identical harvester A of the PVEH achieves a $P_{aggregate-harvester\ A}$ of 200 mW, a 26% improvement. Figure 6 shows the average harvested power of harvester A of the CVEH (Figure 6a) and harvester A of the PVEH (Figure 6b) as a function of excitation frequency and amplitude, with increasing harvested power indicated by increasing brightness. While harvester A of both the PVEH and CVEH exhibits peak performance in a region near the resonant frequency of the unbuckled cantilever ($\frac{1}{2\pi}\sqrt{k_1/m_1}$) (Figures 6a and 6b), harvester A of the PVEH exhibits strong performance over a broader range of excitation conditions. This larger region of strong performance indicates more energetic interwell dynamics for the cantilever are experienced over a broader set of excitation conditions, which can be attributed to the lower potential energy barrier and larger snap through amplitude of harvester A of the PVEH. The broadband average harvested powers of harvester B of the PVEH and harvester C of the CVEH are compared in Figure 7. Harvester B of the PVEH achieves an aggregate power $P_{aggregate-harvester\ B}$ of 217 mW, a 25% enhancement over harvester C of the CVEH, which achieves a $P_{aggregate-harvester\ C}$ of 174 mW. For harvester C of the CVEH, the excitation region of peak performance is narrow, and centered around an excitation frequency of f_e = 5 Hz (Figure 7a). As outlined in a previous study,[39] this performance peak occurs at f_e = 5 Hz because the linear natural frequency of harvester C (f_{n2}) is equal to 10 Hz, and harvester C oscillates at double the frequency of harvester A when the bistable cantilever of harvester A undergoes interwell oscillations. Thus, a 5 Hz excitation frequency results in harvester C oscillating at its natural frequency of 10 Hz, generating linear resonant behavior. From Figure 7b, it is evident that the excitation region of strong performance for harvester B of the PVEH is much larger than that of harvester C of the CVEH. Since harvester B is nonlinear, it does not rely on narrowband linear resonance phenomena to achieve strong performance, and thus can achieve a region of significant harvested power that is more robust to excitation conditions. Therefore, incorporating the asymmetry and nonlinearity into harvester B of the PVEH and achieving bistable dynamics in this subsystem facilitates performance enhancement when compared to the linear harvester C of the CVEH. In summary, incorporating asymmetry and nonlinearity into harvester B of the PVEH enhances the dynamic performance of both subsystems of the PVEH (harvester A and harvester B) and results in substantial enhancement in harvesting capabilities.

5. CONCLUSIONS

In this study, a novel MDOF vibration energy harvester (PVEH) with magnetically coupled bistable modules that can enhance energy harvesting performance through nonlinearity and adaptive potential energy is proposed and investigated. A conventional bistable harvesting element is coupled to an asymmetric nonlinear harvesting element through magnetic interaction. Analysis of the potential energy surface for the system indicates that careful design of the asymmetric nonlinear element can facilitate development of system quad-stability, or multi-directional bistability. Investigation of the quasi-static potential energy trajectory for the device indicates that the asymmetric nonlinear mechanism used to create this potential energy surface enables shaping of the potential energy profiles for both system DOF. Careful selection of the linear stiffness k_2 of the asymmetric nonlinear element allows for the design of potential energy trajectories for both system DOF that maintain large bistable snap-through amplitudes while reducing the potential energy barrier to high energy interwell oscillations. The end result is a quad-stable potential energy surface for the PVEH that is configured to encourage MDOF high amplitude oscillations for a wide range of excitation conditions. Numerical simulations of dynamic response to a large range of practical excitation conditions confirm that the PVEH substantially improves broadband harvesting performance over a system representing the current state of the art (CVEH). Further analysis of the dynamic response suggests that both harvesting elements of the PVEH exhibit highly energetic response for a wide range of excitation conditions, and each provide significant contributions to performance enhancement. The end result is a system with a highly tailorable potential energy profile and rich synergistic dynamics between coupled subsystems, providing amplified peak performance and an enhanced robustness to external excitation conditions.

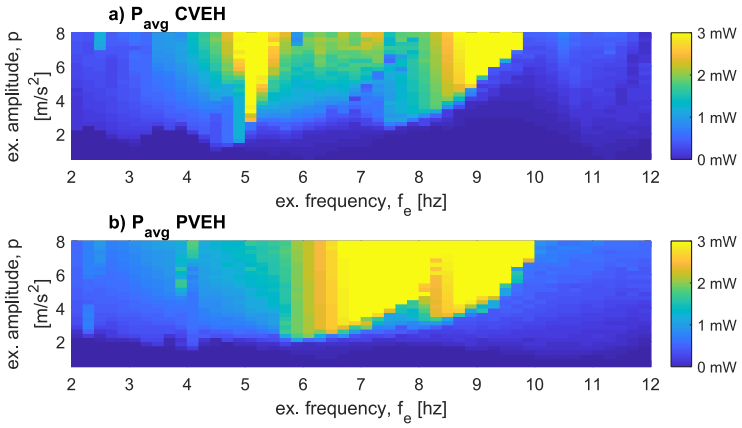

Figure 5. Comparison of average power P_{avg} harvested by entire systems (a) CVEH and (b) PVEH as a function of excitation frequency f_e and excitation amplitude p. More power indicated by increasing brightness.

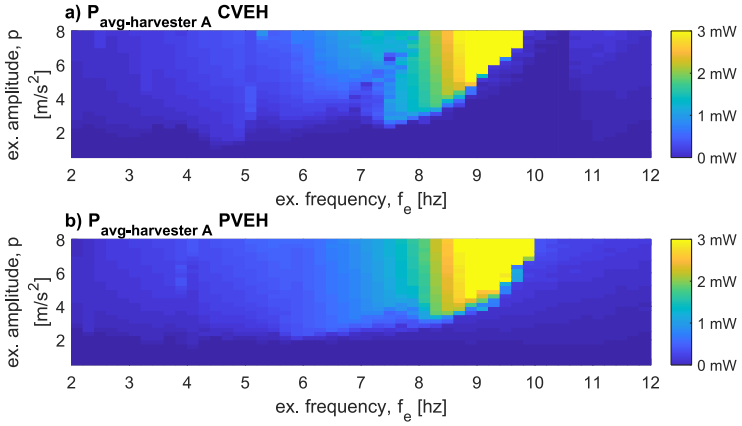

Figure 6. Comparison of average power harvested by (a) harvester A for CVEH and (b) harvester A for PVEH as a function of excitation frequency f_e and excitation amplitude p. More power indicated by increasing brightness.

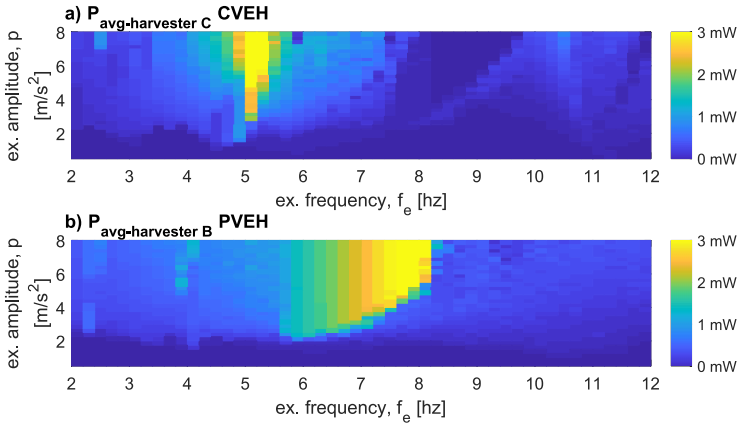

Figure 7. Comparison of average power harvested by (a) harvester C for CVEH and (b) harvester B for PVEH as a function of excitation frequency f_e and excitation amplitude p. More power indicated by increasing brightness.

ACKNOWLEDGEMENTS

This research is funded by the National Science Foundation under Award No. 1661568.

REFERENCES

[1] Roundy, S., Wright, P. K. and Rabaey, J., "A study of low level vibrations as a power source for wireless sensor nodes," Comput. Commun. 26(11), 1131–1144 (2003).

[2] Green, P. L., Papatheou, E. and Sims, N. D., "Energy harvesting from human motion and bridge vibrations: An evaluation of current nonlinear energy harvesting solutions," J. Intell. Mater. Syst. Struct. 24(12), 1494–1505 (2013).

[3] Elvin, N. G., Lajnef, N. and Elvin, A. A., "Feasibility of structural monitoring with vibration powered sensors," Smart Mater. Struct. 15(4), 977–986 (2006).

[4] Karami, M. A. and Inman, D. J., "Linear and nonlinear energy harvesters for powering pacemakers from heart beat vibrations," Proc. SPIE 7977, Act. Passiv. Smart Struct. Integr. Syst., 797703 (2011).

[5] Anton, S. R. and Inman, D. J., "Vibration energy harvesting for unmanned aerial vehicles," Proc. SPIE 6928, Act. Passiv. Smart Struct. Integr. Syst., 692824 (2008).

[6] Erturk, A., Renno, J. M. and Inman, D. J., "Modeling of piezoelectric energy harvesting from an L-shaped beam-mass structure with an application to UAVs," J. Intell. Mater. Syst. Struct. 20(5), 529–544 (2009).

[7] Shahruz, S. M., "Design of mechanical band-pass filters for energy scavenging," J. Sound Vib. 292(3–5), 987–998 (2006).

[8] Wu, Z., Harne, R. L. and Wang, K. W., "Energy harvester synthesis via coupled linear-bistable system with multistable dynamics," J. Appl. Mech. 81(6), 061005 (2014).

[9] Xue, H., Hu, Y. and Wang, Q. M., "Broadband piezoelectric energy harvesting devices using multiple bimorphs with different operating frequencies," IEEE Trans. Ultrason. Ferroelectr. Freq. Control 55(9), 2104–2108 (2008).

[10] Stanton, S. C., McGehee, C. C. and Mann, B. P., "Reversible hysteresis for broadband magnetopiezoelastic energy harvesting," Appl. Phys. Lett. 95(17), 174103 (2009).

[11] Daqaq, M. F., Masana, R., Erturk, A. and Quinn, D. D., "On the role of nonlinearities in vibratory energy harvesting: a critical review and discussion," Appl. Mech. Rev. 66(4), 040801 (2014).

[12] Cottone, F., Vocca, H. and Gammaitoni, L., "Nonlinear energy harvesting," Phys. Rev. Lett. 102(8), 080601 (2009).

[13] Harne, R. L. and Wang, K. W., "A review of the recent research on vibration energy harvesting via bistable systems," Smart Mater. Struct. 22(2), 023001 (2013).

[14] Harne, R. L., Thota, M. and Wang, K. W., "Concise and high-fidelity predictive criteria for maximizing performance and robustness of bistable energy harvesters," Appl. Phys. Lett. 102(5), 053903 (2013).

[15] Mann, B. P., Barton, D. A. and Owens, B. A., "Uncertainty in performance for linear and nonlinear energy harvesting strategies," J. Intell. Mater. Syst. Struct. 23(13), 1451–1460 (2012).

[16] Harne, R. L. and Wang, K. W., "On the fundamental and superharmonic effects in bistable energy harvesting," J. Intell. Mater. Syst. Struct. 25(8), 937–950 (2014).

[17] Dai, Q. and Harne, R. L., "Investigation of direct current power delivery from nonlinear vibration energy harvesters under combined harmonic and stochastic excitations," J. Intell. Mater. Syst. Struct. 29(4), 514–529 (2018).

[18] Cottone, F., Gammaitoni, L., Vocca, H., Ferrari, M. and Ferrari, V., "Piezoelectric buckled beams for random vibration energy harvesting," Smart Mater. Struct. 21(3) (2012).

[19] Friswell, M. I., Ali, S. F., Bilgen, O., Adhikari, S., Lees, A. W. and Litak, G., "Non-linear piezoelectric vibration energy harvesting from a vertical cantilever beam with tip mass," J. Intell. Mater. Syst. Struct. 23(13), 1505–1521 (2012).

[20] Masana, R. and Daqaq, M. F., "Relative performance of a vibratory energy harvester in mono- and bi-stable potentials," J. Sound Vib. 330(24), 6036–6052 (2011).

[21] Harne, R. L. and Wang, K. W., [Harnessing bistable structural dynamics: for vibration control, energy harvesting and sensing], John Wiley & Sons (2017).

[22] Kovacic, I. and Brennan, M. J., [The Duffing equation: nonlinear oscillators and their behavior], John Wiley & Sons (2011).

[23] Stanton, S. C., McGehee, C. C. and Mann, B. P., "Nonlinear dynamics for broadband energy harvesting: investigation of a bistable piezoelectric inertial generator," Phys. D Nonlinear Phenom. 239(10), 640–653 (2010).

[24] Erturk, A., Hoffmann, J. and Inman, D. J., "A piezomagnetoelastic structure for broadband vibration energy harvesting," Appl. Phys. Lett. 94(25), 254102 (2009).
[25] Harne, R. L. and Wang, K. W., "Prospects for nonlinear energy harvesting systems designed near the elastic stability limit when driven by colored noise," J. Vib. Acoust. 136(2), 021009 (2014).
[26] Zhou, S., Cao, J., Inman, D. J., Lin, J., Liu, S. and Wang, Z., "Broadband tristable energy harvester: modeling and experiment verification," Appl. Energy 133, 33–39 (2014).
[27] Kim, P. and Seok, J., "A multi-stable energy harvester: dynamic modeling and bifurcation analysis," J. Sound Vib. 333(21), 5525–5547 (2014).
[28] Zhou, S., Cao, J., Erturk, A. and Lin, J., "Enhanced broadband piezoelectric energy harvesting using rotatable magnets," Appl. Phys. Lett. 102(17), 173901 (2013).
[29] Lan, C. and Qin, W., "Enhancing ability of harvesting energy from random vibration by decreasing the potential barrier of bistable harvester," Mech. Syst. Signal Process. 85, 71–81 (2017).
[30] Hosseinloo, A. H. and Turitsyn, K., "Non-resonant energy harvesting via an adaptive bistable potential," Smart Mater. Struct. 25(1), 015010 (2015).
[31] Ouellette, S. A. and Todd, M. D., "Modulating the bistable potential energy separatrix for augmented broadband vibration energy harvesting," J. Intell. Mater. Syst. Struct. 28(3), 294–306 (2017).
[32] Nguyen, M. S., Yoon, Y. J., Kwon, O. and Kim, P., "Lowering the potential barrier of a bistable energy harvester with mechanically rectified motion of an auxiliary magnet oscillator," Appl. Phys. Lett. 111(25), 253905 (2017).
[33] Li, H. T. and Qin, W. Y., "Prompt efficiency of energy harvesting by magnetic coupling of an improved bi-stable system," Chinese Phys. B 25(11), 110503 (2016).
[34] Shan, G., Wang, D. F., Song, J., Fu, Y. and Yang, X., "A spring-assisted adaptive bistable energy harvester for high output in low-excitation," Microsyst. Technol. 24(9), 3579–3588 (2018).
[35] Harne, R. L. and Wang, K. W., "Axial suspension compliance and compression for enhancing performance of a nonlinear vibration energy harvesting beam system," J. Vib. Acoust. 138(1), 011004 (2016).
[36] Tang, L. and Yang, Y., "A nonlinear piezoelectric energy harvester with magnetic oscillator," Appl. Phys. Lett. 101(9), 094102 (2012).
[37] Leng, Y. G., Gao, Y. J., Tan, D., Fan, S. B. and Lai, Z. H., "An elastic-support model for enhanced bistable piezoelectric energy harvesting from random vibrations," J. Appl. Phys. 117(6), 064901 (2015).
[38] Gao, Y. J., Leng, Y. G., Fan, S. B. and Lai, Z. H., "Performance of bistable piezoelectric cantilever vibration energy harvesters with an elastic support external magnet," Smart Mater. Struct. 23(9), 095003 (2014).
[39] Kim, J., Dorin, P. and Wang, K. W., "Hybrid-bistable vibration energy harvester with adaptive potential well," ASME 2018 Int. Des. Eng. Tech. Conf. Comput. Inf. Eng. Conf. (2018).
[40] Kim, P., Nguyen, M. S., Kwon, O., Kim, Y. J. and Yoon, Y. J., "Phase-dependent dynamic potential of magnetically coupled two-degree-of-freedom bistable energy harvester," Sci. Rep. 6, 34411 (2016).
[41] Zhou, S., Cao, J., Wang, W., Liu, S. and Lin, J., "Modeling and experimental verification of doubly nonlinear magnet-coupled piezoelectric energy harvesting from ambient vibration," Smart Mater. Struct. 24(5), 055008 (2015).
[42] Zou, H. X., Zhang, W. M., Li, W. B., Wei, K. X., Gao, Q. H., Peng, Z. K. and Meng, G., "Design and experimental investigation of a magnetically coupled vibration energy harvester using two inverted piezoelectric cantilever beams for rotational motion," Energy Convers. Manag. 148, 1391–1398 (2017).
[43] Fan, K. Q., Chao, F. B., Zhang, J. G., Wang, W. D. and Che, X. H., "Design and experimental verification of a bi-directional nonlinear piezoelectric energy harvester," Energy Convers. Manag. 86, 561–567 (2014).
[44] Lan, C., Tang, L., Qin, W. and Xiong, L., "Magnetically coupled dual-beam energy harvester: benefit and trade-off," J. Intell. Mater. Syst. Struct. 29(6), 1216–1235 (2017).
[45] Zhu, D. and Beeby, S. P., "A coupled bistable structure for broadband vibration energy harvesting," 2013 Transducers Eurosensors XXVII Proc. 17th Int. Conf. Solid-State Sensors, Actuators Microsystems, IEEE, 446–449 (2013).
[46] Andò, B., Baglio, S., Maiorca, F. and Trigona, C., "Analysis of two dimensional, wide-band, bistable vibration energy harvester," Sensors Actuators, A Phys. 202, 176–182 (2013).
[47] Du Toit, N. E., "Modeling and design of a MEMS piezoelectric vibration energy harvester," Dr. Diss. Massachusetts Inst. Technol. (2005).
[48] Meirovitch, L., [Anlaytical methods in vibrations], MacMillan, New York, New York (1967).
[49] Inman, D. J. and Erturk, A., [Piezoelectric energy harvesting], John Wiley & Sons (2011).

[50] Xu, Z., Shan, X., Chen, D. and Xie, T., “A novel tunable multi-frequency hybrid vibration energy harvester using piezoelectric and electromagnetic conversion mechanisms,” Appl. Sci. 6(1), 10 (2016).
[51] Yung, K. W., Landecker, P. B. and Villani, D. D., “An analytic solution for the force between two magnetic dipoles,” Phys. Sep. Sci. Eng. 9(1), 39–52 (1998).
[52] Daqaq, M. F., “On intentional introduction of stiffness nonlinearities for energy harvesting under white Gaussian excitations,” Nonlinear Dyn. 69(3), 1063–1079 (2012).
[53] Hosseinloo, A. H. and Turitsyn, K., “Fundamental limits to nonlinear energy harvesting,” Phys. Rev. Appl. 4(6), 064009 (2015).